Study on Low-frequency Noise Characteristics of Hydrogen-terminated Diamond FETs

Hongyue Wang, Eddy Simoen, Lei Ge, Chang Liu, Mingsheng Xu, Yijun Shi, Yuebo Liu, Zongqi Cai, Yan Peng, Xiwei Wang and Jinwang Wang

***Abstract*—In this work, the low frequency noise (LFN) characteristics of Hydrogen-terminated diamond FETs are investigated. Both generation-recombination (GR) noise and flicker noise (1/f noise) are found to contribute to the LFN spectrum. The characteristic frequency of f_{01}=0.1 Hz, f_{02}=30 Hz, f_{03}=300 Hz and corresponding effective trap density (N_{eff}) of the GR centers are obtained. By changing the LFN measurement temperature, a trap activation energy level (E_a) of 0.12 eV is extracted from an Arrhenius plot. The dominant mechanism of the 1/f noise for the H-terminated diamond FETs follows the correlated mobility fluctuations (CMF) model. By fitting the experimental data to the CMF model, the trap density and scattering coefficient of the carriers are extracted to be 6.4×10^{20} $eV^{-1}cm^{-3}$ and 4×10^5 V·s/C. At last, the trap density of the H- terminated diamond FETs is compared with other state-of-the-art GaN and Si based devices. A moderate trap density was obtained without any interface optimization, suggesting that H-terminated diamond FETs could be a promising future technology for power electronics.**

***Index Terms*— Hydrogen-terminated, diamond, low frequency noise, FETs, traps, GR noise**

I. Introduction

DIAMOND exhibits ultra-wide band gap, high breakdown electric field, high hole and electron mobilities and excellent thermal conductivity properties, which make it a promising material for logic circuits, high power application and ultraviolet optoelectronic fields[1-4]. Recently, the Hydrogen (H)-terminated diamond field-effect transistors (FETs) were fabricated and reported to show good device performance including high power density [5-7],high operate frequency [8, 9], and high optoelectronic responsivity [10, 11] etc.

So far, a lot of work has been carried out on the fabrication process to improve the H-terminated diamond transistor performance and reliability. Several dielectric materials deposited by different techniques are used to passivate the diamond surface or serve as gate dielectric, such as atomic layer deposition (ALD) Al_2O_3 [12, 13], ALD-HfO_2 [14], sputter deposition (SD) of TiO_2 [15], thermal evaporation of MoO_3 [16], and thermal oxidation TiO_x [17]. It is found that by depositing an Al_2O_3 passivation layer, the sheet carrier concentration and mobility remained almost unchanged at high operation temperature, while the devices without Al_2O_3 layer exhibit an obvious carrier concentration decrease with temperature changing, which means a high density of active traps are located at the H-diamond surface [13, 18]. Several works have studied the H-terminated diamond FET characteristics degradation under hot-carrier stress. The observed changes in threshold voltage (V_{TH}), on-resistance (R_{ON}) and other device characteristics confirm the presence of defects interacting with the carriers during the bias stress. Defects at the gate/diamond interface and/or the whole channel are found [19, 20]. As can be seen from the above studies, the defects have strong effects on the device performance and reliability. However, the details of the defects in the H-terminated diamond have not been well discussed.

The low frequency noise (LFN) spectroscopy is a powerful method for analyzing the electrically active defects in the semiconductor material. Noise related to the charge transport fluctuations originate from carrier mobility fluctuations and occupancy fluctuations of the defects such as interface states, deep level centers, or border traps in the devices [21-23]. So, by analyzing the LFN spectrum, one can estimate the density, energy level, capture cross section, location and other information of defects in the devices [22, 24]. Besides, the device properties such as mobility (μ) [25, 26], threshold voltage (V_{TH}) stability [27] of power transistors and the detectivity (D^*) of phototransistors [28] can be greatly affected by noise behaviors. The LFN measurement would be a guidance for device optimization and understanding the device degradation mechanism. However, as far as we know, the low frequency noise characteristics of H-terminated diamond FETs has not been studied in great detail.

This work was supported by the national natural science Foundation of China (NSFC) under Grant No. 62204060.

Hongyue Wang, Chang Liu, Yijun Shi Yuebo Liu and Zongqi Cai are with the Science and Technology on Reliability Physics and Application of Electronic Component Laboratory, The Fifth Research Institute of Electronics, Ministry of Industry and Information Technology, Guangzhou 510610, China, (e-mail: xd_liuchang@163.com).

Eddy Simoen is with the IMEC, 3001 Leuven, Belgium, and also with the Solid-State Physics Department of Ghent University, Gent, Belgium

Lei Ge, Mingsheng Xu, Yan Peng and Xiwei Wang are with the Institute of Novel Semiconductor Materials and State Key Laboratory of Crystal Materials, Shandong University, Jinan 250100, China (e-mail: xums@sdu.edu.cn).

Jinyan Wang is with the School of Electronics Engineering and Computer Science, Peking University, Beijing 10071, China

In this work, H-terminated diamond FETs are fabricated and the low frequency noise spectrum of the devices are investigated. The basic device characteristics, such as I-V, C-V, carrier concentration and mobility are presented first. After that, both generation-recombination (GR) noise and flicker noise (1/f noise) are found to contribute to the LFN spectrum of H-terminated diamond FETs. The characteristic frequency and corresponding trap density of GR centers are obtained. The LFN spectrum at different temperatures was measured and the energy level of the GR centers is extracted. The dominant mechanism of the 1/f noise for the H-terminated diamond FETs is analyzed. The trap density at the gate/diamond interface and the scattering coefficient to the carriers are evaluated by fitting the experimental data to the correlated mobility fluctuations (CMF) model. At last, the trap density of the H- terminated diamond FETs is compared with other state-of-the-art GaN and Si based devices.

II. Experiment

A schematic of the H-terminated diamond transistors is shown in Fig. 1(a). The devices were fabricated on the high-quality homoepitaxial diamond film with thickness of 80 μm deposited by microwave plasma chemical vapor deposition (Arids-300 type MPCVD system) on a single-crystal diamond substrate from element-six company (4.5 × 4.5 × 0.5 mm^3). Hydrogen plasma treatment was performed on the grown diamond film at 900 ◦C for 15 min to produce 2-D hole gas (2DHG) [10]. Au and Al are employed as ohmic and gate contact, respectively. Details of the fabrication processes have been reported preciously [10]. The gate length L_G, gate–source distance L_{GS}, gate–drain distance L_{GD} and gate width W of the fabricated devices are 3.5 μm, 1 μm, 4.5 μm and 50 μm, respectively.

The transfer curves, output curves, C-V and carrier concentration of a typical device are shown in Fig.1 (b-d). The saturation output current density ($I_{DS,sat}$) and threshold voltage (V_{TH}) of the devices are 80 mA/mm and -0.2 V (defined at a drain current I_D = 1 μA/mm). The drain current on/off ratio and subthreshold slope (SS), which are mainly affected by the interface state properties, were extracted to be around ~10^{11} and 70 mV, indicating a high-quality device interface. The extracted hole density and mobility are 2.3×10^{13} cm^{-2} and 120 $cm^2/V{\cdot}s$, which are among the state-of-the-art H-terminated diamond transistors [29-31]. Considering the low gate current in the transfer curves and the capacitance plateau in the C-V curve at forward bias voltage, a gate dielectric layer is supposed to exist between the Al and diamond surface. To verify that, transmission electron microscopy (TEM) was performed on the sample. The result is shown in Fig. 2. It is obvious that there is an interface layer of 7~8 nm between the Al and diamond surface, which contains O and Al elements ~~by~~ from energy dispersive X-Ray spectroscopy (EDX) analysis. This interface layer ~~also has~~has also been found in other literatures [32-34].

After that, low frequency noise measurements were carried out using an Agilent E4727A in an air ambient condition in the frequency range from 0.1 Hz to 1 kHz.

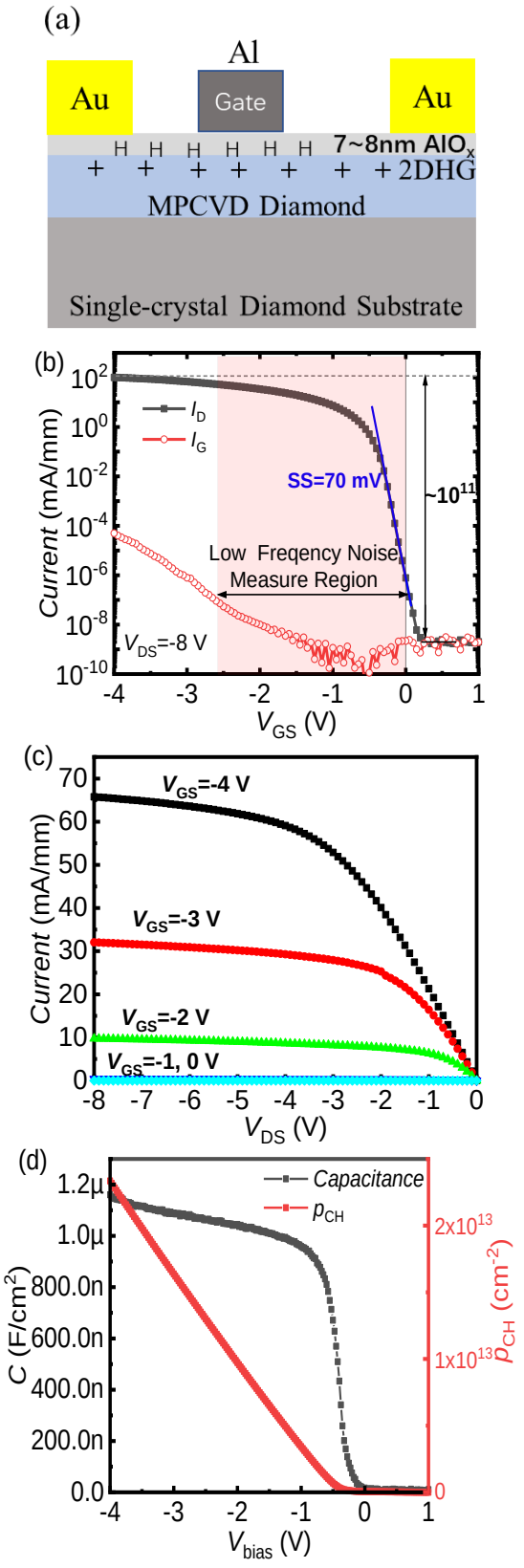

Fig. 1. The (a) device structure schematic, (b) transfer curves in log scale, (c) output characteristics and (d) C-V curves of the gate-source diode and carrier concentration of the H-terminated diamond FETs.

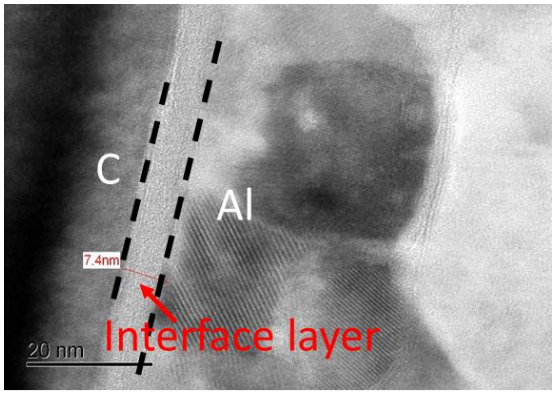

Fig. 2. The transmission electron ~~microscope~~ microscopy image of the H-terminated diamond transistor.

III. Results and Discussion

Figure 3 shows the drain current low frequency noise power spectral density (S_{ID}) versus frequency (f) in log scale corresponding with different gate bias (V_{GS}) at a drain voltage of 0.1 V. S_{ID} increases with the decrease of V_{GS} first and then remains almost constant when V_{GS}<-0.6 V. The dashed straight line in Fig. 3 represents the 1/f slope, which is commonly named as 1/f noise or flicker noise. The overall trend of S_{ID} variation with frequency conforms to 1/f. Besides that, it is obvious that the noise spectra of the H-terminated diamond FETs contain Lorentzian contributions, also known as generation-recombination (GR) noise. The frequency dependence of the different contributions on the total noise S_{ID} can be written as follows [35, 36]:

$$S_{ID}(f) = B + K_f/f + \sum_{i=1}^{N} \frac{A_{0i}}{1+\left(\frac{f}{f_{0i}}\right)^2} \qquad (1)$$

where B is related to the white noise level, K_f/f represents the flicker noise and the third term of the equation presents a sum of Lorentzian components, with A_{0i} the plateau value and f_{0i} the characteristic frequency, corresponding with the peak value in the $f \times S_{ID}$ plot.

In order to ~~have a clear~~clearly see each Lorentzian contribution, the frequency normalized S_{ID} ($f \times S_{ID}$) relation with frequency is calculated and the raw data and smoothed curves are shown in Fig_.4. It is found that when $|V_{GS}|$<0.25 V, two Lorentzian contributions GR1 and GR2 are found located at a frequency ~~of~~ f_{01}= 300 Hz and f_{02}≤0.1 Hz, respectively. When $|V_{GS}|$>0.3 V, another Lorentzian contribution GR3 with characteristic frequency f_{03} at around 30 Hz begins to appear and the amplitude of which increases with $|V_{GS}|$ increasing. One can observe that the f_{01} and f_{03} are constant with $|V_{GS}|$ increasing, suggesting that the related GR traps are in the diamond layer (depletion region), and not in the gate stack [37]. ~~And b~~On the other hand, because of the low frequency limit of the equipment, the accurate peak location of GR2 cannot be determined.

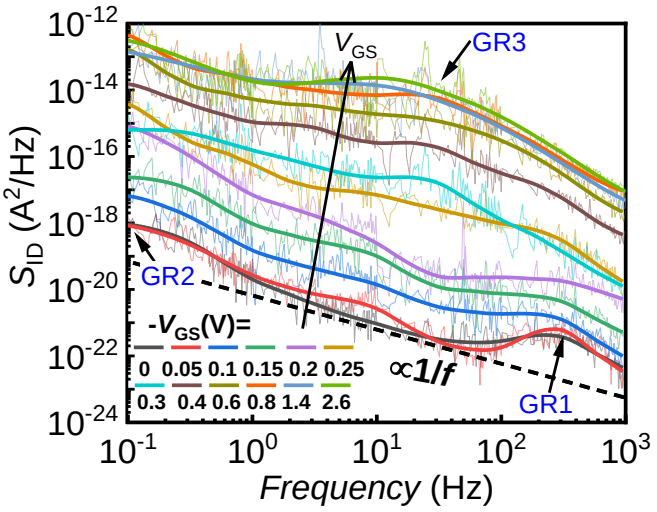

Fig. 3. Drain current power spectral density S_{ID} corresponding with different V_{GS} in the ohmic regime.

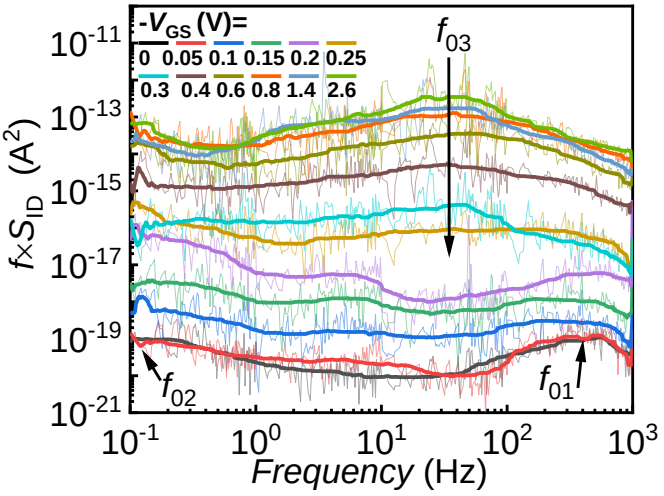

Fig. 4. Frequency normalized spectra $f \times S_{ID}$ derived from Fig. 3.

A. G-R contributions

To distinguish the 1/f and G-R contributions, the total noise model expressed by equation (1) is used to fit the experimental results. The fitting curves at two representative voltages of V_{GS}=0 V and -0.8 V are shown in Fig. 5. It can be seen that the experimental results are well fitted by the total noise model. The A_{0i} and corresponding f_{0i} as a function of V_{GS} are shown in Fig.6. The A_{0i} of all three GR centers first increases with the increase of $|V_{GS}|$, and then shows a plateau. The effective trap density (N_{eff}) for the GR centers in the diamond channel can be estimated from:

$$A_{0i} = \frac{q^2 g_m{}^2 N_{eff}}{WLC_{acc}{}^2}\tau_{0i}, \qquad (2)$$

where g_m is the transconductance in each operation point, τ_{0i} is the GR center relaxation time constant that is defined as $1/(2\pi f_{0i})$, q is the elementary charge, W and L is the device width and gate length, C_{acc} is the capacitance in accumulation [38]. The effective trap density of the three GR centers changes with $|V_{GS}|$ as shown in Fig.6 (b). It can be observed that GR1 shows a low N_{eff} of ~10^{12} cm^{-2}. The N_{eff} of GR2 and GR3 gradually increases with V_{GS}, indicating an increase of the trap density with decreasing Fermi level at the gate/diamond

interface. This phenomenon is also found in GaN devices [39]. The obtained maximum N_{eff} values of GR2 and GR3 are around 10^{18} and 10^{19} cm^{-2}.

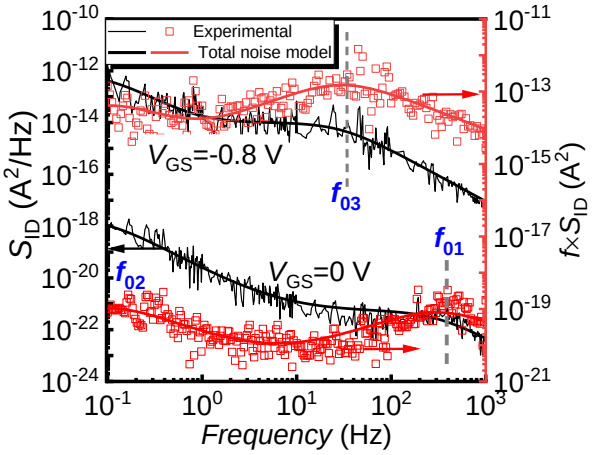

Fig. 5. The experimental and fitting curves of total noise model for S_{ID} and $f\times S_{ID}$ at two representative voltages of V_{GS}=0 V and -0.8V.

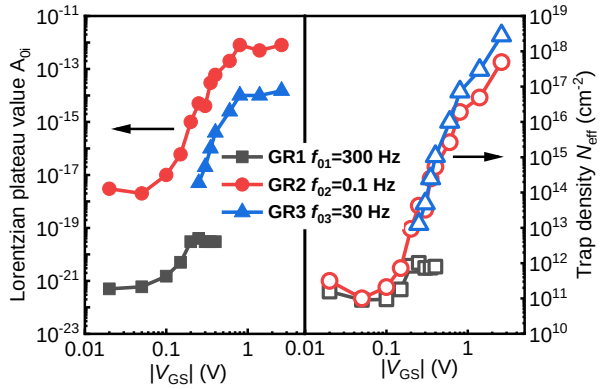

Fig. 6. (a) Lorentzian plateau value and (b) effective trap density of three GR centers changing with |V_{GS}|.

The relaxation time constant τ_{0i} changes with temperature T as according to the Arrhenius law:

$$\tau_{0i} = \frac{\exp\left(\frac{E_T - E_V}{kT}\right)}{\gamma_h \sigma_h T^2} \qquad (3)$$

where $\gamma_h = (v_{th}/T^{1/2})(N_V/T^{3/2})$, v_{th} is the mean thermal velocity, N_V is the effective states density in the valence band, and σ_h is the hole capture cross section. T is the absolute temperature and k is Boltzmann's constant. From the slope of the evolution of $\ln(\tau_{0i}T^2)$ versus $1/(kT)$ one can extract the trap activation energy E_A=E_T-E_V. The physical nature of these traps can be identified by comparing the energy and capture cross section of the traps with data in the literature.

The $f\times S_{ID}$ curves at V_{GS}=-0.1V with different temperature are shown in Fig. 7. Because the f_{02} is below the measurement minimum frequency limit, and the f_{03} is strongly influenced by the GR1 and GR2 leading to a broad peak, the exact characteristic frequency of them cannot be obtained. So, only the f_{01} change with T of GR1 is performed. The Arrhenius diagram of GR1 is plotted in Fig. 8. An activation energy E_A of 0.12 eV is derived, which may relate to the H impurities in the diamond. The origin of the GR1 needs to be further investigated by first principles calculations and other methods.

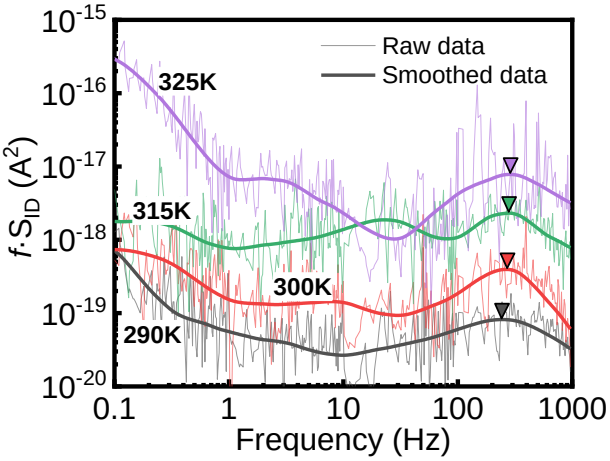

Fig. 7. Frequency normalized noise spectral density versus temperature for the H-terminated diamond FETs.

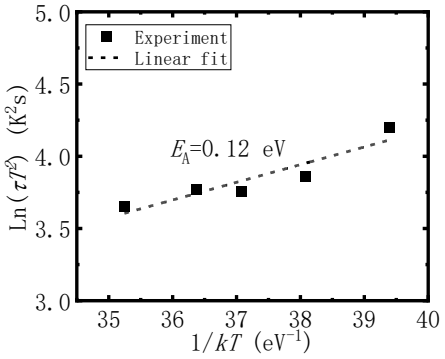

FIG. 8 Arrhenius plots of the GR1 trap.

B. 1/f noise characteristics

By subtracting the Lorentzion contributions from the S_{ID}, the 1/f noise curves are obtained. The 1/f noise fluctuation mechanism in the H-terminated diamond FETs is discussed.

Three theories are proposed to explain the 1/f noise, namely carrier number fluctuations (CNF), Hooge mobility fluctuations (HMF) and correlated mobility fluctuations (CMF)[40] . In the theory of carrier number fluctuations, which is proposed by McWhorter in 1957 , the 1/f noise stems from the random trapping and detrapping processes of charges near the conduction interface [41]. The normalized noise power spectral density(S_{ID}/I_D^2) follows:

$$\frac{S_{ID}}{I_D^2} = \frac{g_m^2}{I_D^2} \cdot S_{Vfb} \qquad (4)$$

where g_m is the transconductance, and S_{Vfb} is the flatband voltage spectral density. By extension, the correlated mobility fluctuations (CMF) contain the influence of the trapping induced change on the mobility, associated with CNF, given by:

$$\frac{S_{ID}}{I_D^2} = \left[1 + \alpha\mu_{eff}C_{ox}\frac{I_D}{g_m}\right]^2 \frac{g_m^2}{I_d^2} \cdot S_{Vfb} \qquad (5)$$

where α is the scattering coefficient, μ_{eff} is the effective mobility, and C_{ox} is the inversion capacitance density of the gate dielectric. Assuming elastic tunneling to traps uniformly

distributed in the gate dielectric [42], the S_{Vfb} is defined by:

$$S_{Vfb} = \frac{q^2 kT\lambda N_T}{WLC_{ox}^2 f} \qquad (6)$$

where q is the elementary charge , λ is the attenuation tunneling parameter taken as 1×10^{-8} cm^{-1}, N_T is the trap density in the gate dielectric[43]. The trapping and detrapping processes of channel carriers influence the flat band voltage as described by the equation of S_{Vfb}.

In combination with the equation of S_{ID}, the relationship between S_{ID} and input referred gate noise spectra (S_{Vg}) can be equated as:

$$S_{Vg} = \frac{S_{ID}}{g_m^2} = \left[1 + \alpha\mu_{eff}C_{ox}\frac{I_D}{g_m}\right]^2 \cdot S_{Vfb} \qquad (7)$$

At strong inversion, S_{Vg} can evolve into :

$$S_{Vg} = \left[1 + \alpha\mu_{eff}C_{ox}(V_{GS} - V_{TH})\right]^2 \cdot S_{Vfb} \qquad (8)$$

On the other hand, the HMF model, proposed by Hooge, is related to intrinsic mobility fluctuations due to phonon scattering probability fluctuations [44]. In the ohmic regime at a drain voltage of 0.1 V, with the increase of V_{GS}, according to Hooge's empirical model the equation of S_{ID} can be expressed as:

$$S_{ID} = \frac{\alpha_H I_D^2}{fN} \qquad (9)$$

where α_H is the Hooge parameter, N is the total number of carriers in the channel; the value of α_H can be utilized as a parameter to compare the quality of channel materials with respect to their susceptibility for generating LFN. The Hooge parameter indicates the bulk effect which is relevant to the manufacturing process of devices. In the strong inversion region, the total number of carriers in the channel follows:

$$N = \frac{|V_{GS} - V_{TH}|}{q} \cdot C_{ox} \qquad (10)$$

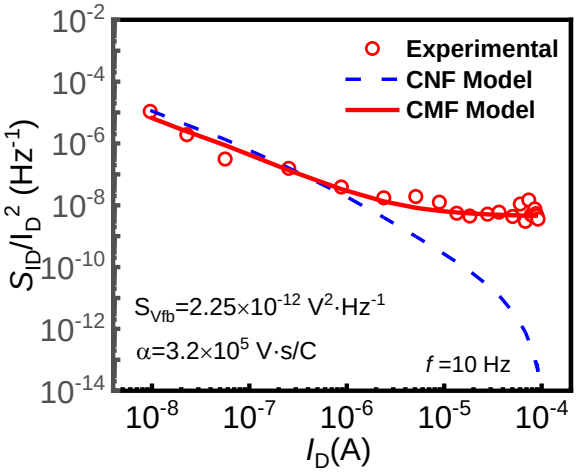

FIG. 9 Comparison between experimental normalized drain current noise S_{ID}/I_D^2 versus I_D at 10 Hz with fitted CNF model and CMF model.

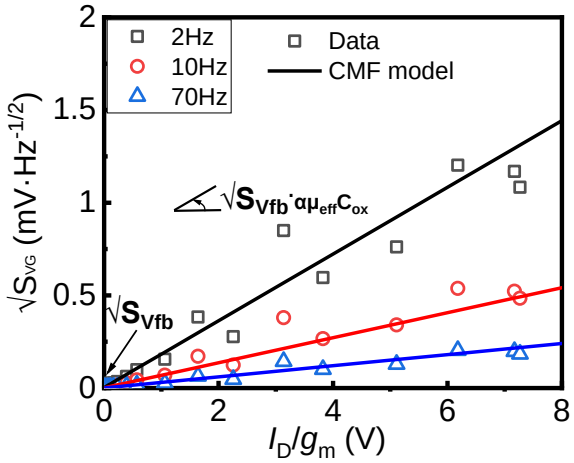

FIG. 10 Plot of $\sqrt{s_{vG}}$ versus I_D/g_m with experimental data and CMF model fitting.

The S_{ID}/I_D^2 versus I_D curves at 10 Hz are shown in Fig.9. The comparison between experimental normalized drain current noise S_{ID}/I_D^2 versus I_D with CNF model and CMF model is also demonstrated. Obviously, the CMF model accounts well for the noise variation across the whole range of current. In this way, data points at a frequency of 2 Hz, 10 Hz and 70 Hz are analyzed by the CMF model. Through fitting the plot of $\sqrt{S_{VG}}$ versus I_D/g_m by Eq. (8), S_{Vfb} and α are extracted and shown in Table I. The α value is around 4×10^5 V·s/C, which is slightly higher than observed in GaN (9.2×10^4 V·s/C) [45] and Si (6×10^3~3×10^4 V·s/C) [46] based devices.

Table 1. The value of S_{Vfb} and α at different frequency

Frequency	S_{Vfb} (V^2·Hz^{-1})	α (Vs/C)	N_T ($eV^{-1}cm^{-3}$)
2Hz	9×10^{-12}	4.31×10^5	6×10^{20}
10 Hz	2.25×10^{-12}	3.23×10^5	7.5×10^{20}
70 Hz	2.5×10^{-13}	4.31×10^5	5.8×10^{20}

And then the trap density N_T calculated using Equation (6) is around 6.4×10^{20} $eV^{-1}cm^{-3}$. To have a clear comparation with other semiconductor devices, a benchmark of the trap density of H-terminated diamond FETs and various state-of-art GaN [39, 45, 47-50] and silicon CMOS [36, 46, 51] technologies reported in the literature is shown in Fig.11 . The N_T obtained in this study is comparable to some previously reported GaN devices on sapphire substrate, suggesting that H-terminated diamond FETs could be a promising future technology. However, the N_T obtained in this study is worse than the carefully optimized GaN devices and Si CMOS devices, indicating further improvement on the interface quality of H-diamond/gate metal and diamond surface is necessary for performance improvement and high device reliability. Passivation and surface treatment of diamond devices are still the one of the most important issues that determine their engineering applications.

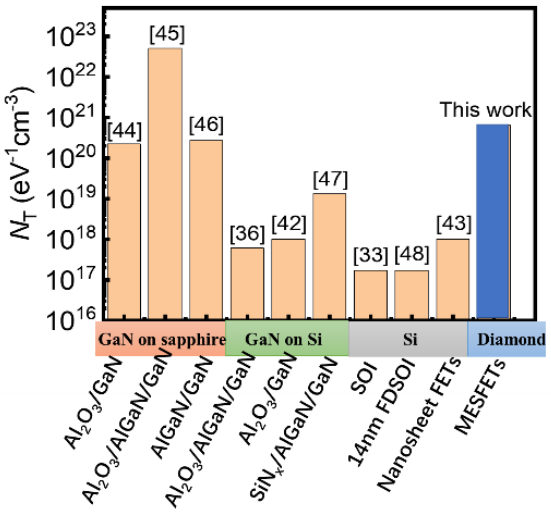

FIG. 11 Benchmarking of the mean trap density (N_T) for H-terminated diamond FETs of this work with state-of-the-art GaN-based, FDSOI and CMOS technologies

IV. Conclusion

In conclusion, the low frequency noise characteristics of the H-terminated diamond FETs are investigated. Both generation-recombination (GR) noise and flicker noise (1/f noise) are found to contribute to the LFN spectrum. Three GR contributions are found with characteristic frequency of f_{01}<0.1 Hz, f_{02}=30 Hz, f_{03}=300 Hz. The corresponding effective trap density of the GR contributions are obtained. By changing the LFN measurement temperature, a trap activation energy level of 0.12 eV is extracted from an Arrhenius plot. The 1/f noise for the H-terminated diamond FETs can be described by the correlated mobility fluctuations model. In addition, the model parameters, N_T and α, are extracted to be 6.4×10^{20} eV^{-1}cm^{-3} and 4×10^{5} V·s/C. The N_T obtained in this study is comparable to some previously reported GaN devices on sapphire substrate, but worse than the carefully optimized GaN devices and Si CMOS devices. Further passivation to the surface is preferred to improve the device performance of the H-terminated diamond FETs.

References

[1] M. W. Geis, T. C. Wade, C. H. Wuorio, T. H. Fedynyshyn, B. Duncan, M. E. Plaut, J. O. Varghese, S. M. Warnock, S. A. Vitale, and M. A. Hollis, Progress Toward Diamond Power Field-Effect Transistors, physica status solidi (a) 215 (22) (2018) 1800681, https://doi.org/10.1002/pssa.201800681.

[2] Y. Sasama, T. Kageura, M. Imura, K. Watanabe, T. Taniguchi, T. Uchihashi, and Y. Takahide, High-mobility p-channel wide-bandgap transistors based on hydrogen-terminated diamond/hexagonal boron nitride heterostructures, Nature Electronics 5 (1) (2022) 37-44, https://doi.org/10.1038/s41928-021-00689-4.

[3] J. S. Lundh, D. Shoemaker, A. G. Birdwell, J. D. Weil, L. M. De La Cruz, P. B. Shah, K. G. Crawford, T. G. Ivanov, H. Y. Wong, and S. Choi, Thermal performance of diamond field-effect transistors, Applied Physics Letters 119 (14) (2021) 143502, https://doi.org/10.1063/5.0061948.

[4] J. Liu, H. Ohsato, M. Liao, M. Imura, E. Watanabe, and Y. Koide, Logic Circuits With Hydrogenated Diamond Field-Effect Transistors, IEEE Electron Device Letters 38 (7) (2017) 922-925, https://doi.org/10.1109/LED.2017.2702744.

[5] R. Soleimanzadeh, M. Naamoun, R. A. Khadar, R. v. Erp, and E. Matioli, H-Terminated Polycrystalline Diamond p-Channel Transistors on GaN-on-Silicon, IEEE Electron Device Letters 41 (1) (2020) 119-122, https://doi.org/10.1109/LED.2019.2953245.

[6] K. Hirama, H. Sato, Y. Harada, H. Yamamoto, and M. Kasu, Diamond Field-Effect Transistors with 1.3 A/mm Drain Current Density by Al2O3 Passivation Layer, Japanese Journal of Applied Physics 51 (9R) (2012) 090112, https://dx.doi.org/10.1143/JJAP.51.090112.

[7] Y. T. Lee, A. Vardi, and M. Tordjman, A hybrid self-aligned MIS-MESFET architecture for improved diamond-based transistors, Applied Physics Letters 117 (20) (2020) 202101, https://doi.org/10.1063/5.0023662.

[8] S. Russell, S. Sharabi, A. Tallaire, and D. A. J. Moran, RF Operation of Hydrogen-Terminated Diamond Field Effect Transistors: A Comparative Study, IEEE Transactions on Electron Devices 62 (3) (2015) 751-756, https://doi.org/10.1109/TED.2015.2392798.

[9] X. Yu, J. Zhou, C. Qi, Z. Cao, Y. Kong, and T. Chen, A High Frequency Hydrogen-Terminated Diamond MISFET With ${f}_{{\text{T}}}/{f}_{\max}$ of 70/80 GHz, IEEE Electron Device Letters 39 (9) (2018) 1373-1376, https://doi.org/10.1109/LED.2018.2862158.

[10] L. Ge, Y. Peng, B. Li, X. Chen, M. Xu, X. Wang, Y. Cui, D. Wang, J. Han, K. Y. Cheong, P. Tanner, M. Zhao, and X. Xu, A Highly Responsive Hydrogen-Terminated Diamond-Based Phototransistor, IEEE Electron Device Letters 43 (8) (2022) 1271-1274, https://doi.org/10.1109/LED.2022.3180845.

[11] Y.-J. Lu, C.-N. Lin, and C.-X. Shan, Optoelectronic Diamond: Growth, Properties, and Photodetection Applications, Advanced Optical Materials 6 (20) (2018) 1800359, https://doi.org/10.1002/adom.201800359.

[12] Z. Chen, X. Yu, J. Zhou, S. Mao, Y. Fu, B. Yan, R. Xu, Y. Kong, T. Chen, Y. Li, and Y. Xu, Negative constant voltage stress-induced threshold voltage instability in hydrogen-terminated diamond MOSFETs with low-temperature deposited Al2O3, Applied Physics Letters 117 (13) (2020) 133501, https://doi.org/10.1063/5.0020136.

[13] M. Kasu, H. Sato, and K. Hirama, Thermal Stabilization of Hole Channel on H-Terminated Diamond Surface by Using Atomic-Layer-Deposited Al2O3 Overlayer and its Electric Properties, Applied Physics Express 5 (2) (2012) 025701, https://dx.doi.org/10.1143/APEX.5.025701.

[14] J. W. Liu, M. Y. Liao, M. Imura, and Y. Koide, Normally-off HfO2-gated diamond field effect transistors, Applied Physics Letters 103 (9) (2013) 092905, https://doi.org/10.1063/1.4820143.

[15] J. W. Liu, M. Y. Liao, M. Imura, R. G. Banal, and Y. Koide, Deposition of TiO2/Al2O3 bilayer on hydrogenated diamond for electronic devices: Capacitors, field-effect transistors, and logic inverters, Journal of Applied Physics 121 (22) (2017) 224502, https://doi.org/10.1063/1.4985066.

[16] Z. Ren, J. Zhang, J. Zhang, C. Zhang, S. Xu, Y. Li, and Y. Hao, Diamond Field Effect Transistors With MoO3 Gate Dielectric, IEEE Electron Device Letters 38 (6) (2017) 786-789, https://doi.org/10.1109/LED.2017.2695495.

[17] M. Zhang, W. Wang, G. Chen, H. N. Abbasi, Y. Wang, F. Lin, F. Wen, K. Wang, J. Zhang, R. Bu, and H. Wang, Normally Off Hydrogen-Terminated Diamond Field-Effect Transistor With Ti/TiOx Gate Materials, IEEE Transactions on Electron Devices 67 (11) (2020) 4784-4788, https://doi.org/10.1109/TED.2020.3025515.

[18] A. Daicho, T. Saito, S. Kurihara, A. Hiraiwa, and H. Kawarada, High-reliability passivation of hydrogen-terminated diamond surface by atomic layer deposition of Al2O3, Journal of Applied Physics 115 (22) (2014) 223711, https://doi.org/10.1063/1.4881524.

[19] C. D. Santi, L. Pavanello, A. Nardo, C. Verona, G. V. Rinati, D. Cannatà, F. D. Pietrantonio, G. Meneghesso, E. Zanoni, and M. Meneghini, Cause and Effects of OFF-State Degradation in Hydrogen-Terminated Diamond MESFETs, IEEE Transactions on Electron Devices 67 (10) (2020) 4021-4026, https://doi.org/10.1109/TED.2020.3019018.

[20] C. De Santi, L. Pavanello, A. Nardo, C. Verona, G. Verona Rinati, G. Meneghesso, E. Zanoni, and M. Meneghini, Reliability of H-terminated diamond MESFETs in high power dissipation operating condition, Microelectronics Reliability 114 (2020) 113898, https://doi.org/10.1016/j.microrel.2020.113898.

[21] L. Pichon, A. Boukhenoufa, C. Cordier, and B. Cretu, Determination of interface state distribution in polysilicon thin film transistors from low-frequency noise measurements: Application to analysis of electrical properties, Journal of Applied Physics 100 (5) (2006) 054504, https://doi.org/10.1063/1.2335395.

[22] M. Silvestri, M. J. Uren, N. Killat, D. Marcon, and M. Kuball, Localization of off-stress-induced damage in AlGaN/GaN high electron mobility transistors by means of low frequency 1/f noise measurements, Applied Physics Letters 103 (4) (2013) 043506, https://doi.org/10.1063/1.4816424.

[23] A. V. Oliveira, E. Simoen, J. Mitard, P. G. D. Agopian, J. A. Martino, R. Langer, L. J. Witters, N. Collaert, A. Thean, and C. Claeys, GR-Noise Characterization of Ge pFinFETs With STI First and STI Last Processes, IEEE Electron Device Letters 37 (9) (2016) 1092-1095, https://doi.org/10.1109/LED.2016.2595398.

[24] X. S. Nguyen, K. Lin, Z. Zhang, B. McSkimming, A. R. Arehart, J. S. Speck, S. A. Ringel, E. A. Fitzgerald, and S. J. Chua, Correlation of a generation-recombination center with a deep level trap in GaN, Applied Physics Letters 106 (10) (2015) 102101, https://doi.org/10.1063/1.4914393.

[25] A. V. d. Oliveira, D. Xie, H. Arimura, G. Boccardi, N. Collaert, C. Claeys, N. Horiguchi, and E. Simoen, Low-Frequency Noise Characterization of Germanium n-Channel FinFETs, IEEE Transactions on Electron Devices 67 (7) (2020) 2872-2877, https://doi.org/10.1109/TED.2020.2990714.

[26] H.-S. Choi, S. Jeon, H. Kim, J. Shin, C. Kim, and U. I. Chung, The impact of active layer thickness on low-frequency noise characteristics in InZnO thin-film transistors with high mobility, Applied Physics Letters 100 (17) (2012) 173501, https://doi.org/10.1063/1.4705406.

[27] H. S. Choi, S. Jeon, H. Kim, J. Shin, C. Kim, and U. I. Chung, Verification of Interface State Properties of a-InGaZnO Thin-Film Transistors With $\hbox{SiN}_{x}$ and $ \hbox{SiO}_{2}$ Gate Dielectrics by Low-Frequency Noise Measurements, IEEE Electron Device Letters 32 (8) (2011) 1083-1085, https://doi.org/10.1109/LED.2011.2158057.

[28] J. Kim, M. G. Kim, A. Facchetti, and S. K. Park, Analysis of Low-Frequency Noise in Quantum Dot/Metal-Oxide Phototransistors With Metal Chalcogenide Interfaces, IEEE Electron Device Letters 43 (9) (2022) 1499-1502, https://doi.org/10.1109/LED.2022.3189605.

[29] H. Kawarada, H. Tsuboi, T. Naruo, T. Yamada, D. Xu, A. Daicho, T. Saito, and A. Hiraiwa, C-H surface diamond field effect transistors for high temperature (400 °C) and high voltage (500 V) operation, Applied Physics Letters 105 (1) (2014) 013510, https://doi.org/10.1063/1.4884828.

[30] J. J. Wang, Z. Z. He, C. Yu, X. B. Song, H. X. Wang, F. Lin, and Z. H. Feng, Comparison of field-effect transistors on polycrystalline and single-crystal diamonds, Diamond and Related Materials 70 (2016) 114-117, https://doi.org/10.1016/j.diamond.2016.10.016.

[31] Y. Li, J.-F. Zhang, G.-P. Liu, Z.-Y. Ren, J.-C. Zhang, and Y. Hao, Mobility of Two-Dimensional Hole Gas in H-Terminated Diamond, physica status solidi (RRL) – Rapid Research Letters 12 (3) (2018) 1700401, https://doi.org/10.1002/pssr.201700401.

[32] A. Kubovic, A. Denisenko, W. Ebert, M. Kasu, I. Kallfass, and E. Kohn, Electronic surface barrier characteristics of H-terminated and surface conductive diamond, Diamond and related materials 13 (4-8) (2004) 755-760, https://doi.org/10.1016/j.diamond.2003.12.004.

[33] M. Kasu, K. Ueda, H. Kageshima, and Y. Yamauchi, Gate interfacial layer in hydrogen-terminated diamond field-effect transistors, Diamond and Related Materials 17 (4) (2008) 741-744, https://doi.org/10.1016/j.diamond.2007.12.022.

[34] F. Maier, M. Riedel, B. Mantel, J. Ristein, and L. Ley, Origin of Surface Conductivity in Diamond, Physical Review Letters 85 (16) (2000) 3472-3475, https://doi.org/10.1103/PhysRevLett.85.3472.

[35] A. Ziel, Noise in Solid State Devices and Circuits, (1986) https://doi.org/10.1016/S0065-2539(08)60414-X.

[36] S. D. dos Santos, B. Cretu, V. Strobel, J. M. Routoure, R. Carin, J. A. Martino, M. Aoulaiche, M. Jurczak, E. Simoen, and C. Claeys, Low-frequency noise assessment in advanced UTBOX SOI nMOSFETs with different gate dielectrics, Solid-State Electronics 97 (2014) 14-22, https://doi.org/10.1016/j.sse.2014.04.034.

[37] S. Christensson, I. Lundström, and C. Svensson, Low frequency noise in MOS transistors—I Theory, Solid-State Electronics 11 (9) (1968) 797-812, https://doi.org/10.1016/0038-1101(68)90100-7.

[38] N. Lukyanchikova and A. Balandin, Sources of the Lorentzian components in the low-frequency noise spectra of submicron metal-oxide-semiconductor field-effect transistors, Noise and fluctuations control in electronic devices (2002) 201-233, https://doi.org/10.1142/S0219477503001154.

[39] K. Takakura, V. Putcha, E. Simoen, A. R. Alian, U. Peralagu, N. Waldron, B. Parvais, and N. Collaert, Low-Frequency Noise Investigation of GaN/AlGaN Metal–Oxide–Semiconductor High-Electron-Mobility Field-Effect Transistor With Different Gate Length and Orientation, IEEE Transactions on Electron Devices 67 (8) (2020) 3062-3068, https://doi.org/10.1109/TED.2020.3002732.

[40] G. Ghibaudo and J. Chroboczek, On the origin of the LF noise in Si/Ge MOSFETs, Solid-State Electronics 46 (3) (2002) 393-398, https://doi.org/10.1016/S0038-1101(01)00112-5.

[41] G. Ghibaudo, O. Roux, C. Nguyen-Duc, F. Balestra, and J. Brini, Improved Analysis of Low Frequency Noise in Field-Effect MOS Transistors, physica status solidi (a) 124 (2) (1991) 571-581, https://doi.org/10.1002/pssa.2211240225.

[42] J. Rhayem, D. Rigaud, M. Valenza, N. Szydlo, and H. Lebrun, 1/f noise modeling in long channel amorphous silicon thin film transistors, Journal of Applied Physics 87 (4) (2000) 1983-1989, https://doi.org/10.1063/1.372124.

[43] R. Jayaraman and C. G. Sodini, A 1/f noise technique to extract the oxide trap density near the conduction band edge of silicon, IEEE Transactions on Electron Devices 36 (9) (1989) 1773-1782, https://doi.org/10.1109/16.34242.

[44] F. N. Hooge, T. G. M. Kleinpenning, and L. K. J. Vandamme, Experimental studies on 1/f noise, Reports on Progress in Physics 44 (5) (1981) 479, https://dx.doi.org/10.1088/0034-4885/44/5/001.

[45] R. K. Kammeugne, C. Theodorou, C. Leroux, X. Mescot, L. Vauche, R. Gwoziecki, S. Becu, M. Charles, E. Bano, and G. Ghibaudo, Thorough Investigation of Low Frequency Noise Mechanisms in AlGaN/GaN and Al2O3/GaN HEMTs, in *2021 IEEE International Electron Devices Meeting (IEDM)*, 2021, pp. 39.4.1-39.4.4, https://doi.org/10.1109/IEDM19574.2021.9720522.

[46] A. Oliveira, A. Veloso, C. Claeys, N. Horiguchi, and E. Simoen, Low-Frequency Noise Assessment of Vertically Stacked Si n-Channel Nanosheet FETs With Different Metal Gates, IEEE Transactions on Electron Devices 67 (11) (2020) 4802-4807, https://doi.org/10.1109/TED.2020.3024271.

[47] K. S. Im, S. J. An, C. G. Theodorou, G. Ghibaudo, S. Cristoloveanu, and J. H. Lee, Effect of Gate Structure on the Trapping Behavior of GaN Junctionless

FinFETs, IEEE Electron Device Letters 41 (6) (2020) 832-835, https://doi.org/10.1109/LED.2020.2991164.

[48] S. Vodapally, C. G. Theodorou, Y. Bae, G. Ghibaudo, S. Cristoloveanu, K. S. Im, and J. H. Lee, Comparison for 1/ ${f}$ Noise Characteristics of AlGaN/GaN FinFET and Planar MISHFET, IEEE Transactions on Electron Devices 64 (9) (2017) 3634-3638, https://doi.org/10.1109/TED.2017.2730919.

[49] Y.-J. Choi, J.-H. Lee, J.-S. Choi, S.-J. An, Y.-M. Hwang, J.-S. Roh, and K.-S. Im, Improved Noise and Device Performances of AlGaN/GaN HEMTs with In Situ Silicon Carbon Nitride (SiCN) Cap Layer, Crystals 11 (5) (2021) https://doi.org/10.3390/cryst11050489.

[50] Z. He, Y. Chen, J. He, W. Su, W. Fang, Y. En, Y. Huang, and Y. Liu, Hydrogen effects on AlGaN/GaN MISFET with LPCVD-SiNx gate dielectric, Semiconductor Science and Technology 34 (3) (2019) 035020, https://dx.doi.org/10.1088/1361-6641/ab00c7.

[51] E. G. Ioannidis, S. Haendler, A. Bajolet, J. Rosa, J. P. Manceau, C. A. Dimitriadis, and G. Ghibaudo, Evolution of low frequency noise and noise variability through CMOS bulk technology nodes, in *2013 22nd International Conference on Noise and Fluctuations (ICNF)*, 2013, pp. 1-4, https://doi.org/10.1109/ICNF.2013.6578985.